Applied Mathematics and Computation 293 (2017) 600–610

Contents lists available at ScienceDirect

Applied Mathematics and Computation

journal homepage: www.elsevier.com/locate/amc

Compressible dusty gas along a vertical wavy surface

Sadia Siddiqa[a,*], Naheed Begum[b], Md. Anwar Hossain[c]

[a] Department of Mathematics, COMSATS Institute of Information Technology, Kamra Road, Attock, Pakistan
[b] Institute of Applied Mathematics (LSIII), TU Dortmund, Vogelpothsweg 87, D-44221 Dortmund, Germany
[c] Department of Mathematics, University of Dhaka, Dhaka, Bangladesh

ARTICLE INFO

Keywords:
Natural convection
Two-phase
Compressible dusty fluid
Wavy surface

ABSTRACT

This analysis deals with the numerical solutions for the compressible natural convection flow of two-phase dusty gas. In particular, it gives the solutions for the flow having spherical particles suspended in the gas (air) over the surface with sharp lateral curvatures. The governing equations are converted into dimensionless equations by using a set of suitable continuous transformations and solved through the implicit finite difference method. The effect of compressibility, dusty gas and sinusoidal waveform are discussed in detail in terms of local heat transfer rate, skin friction coefficient, velocity and temperature distributions. This investigation reveals the fact that the air–particle mixture reduces the rate of heat transfer, significantly.

1. Introduction

Compressible fluid flows are of great importance in mechanical, aerospace and chemical engineering problems and the understanding of the influence of compressibility on the flow formation comes out to be a much needed information in this context. The most obvious applications of compressible fluid flow theory are found in the design of aircrafts and also in the design and operation of devices used in gas turbines, reciprocating engines, stream turbines, natural gas transmission lines and combustion chambers [1]. For high Reynolds number, the problem of compressible laminar boundary layer flow along a flat surface has been studied by Kuerti [2] and Young [3]. Moore [4] developed the first-order deviations of the velocity and temperature distributions for the compressible, quasi-steady state, boundary layer flow over a semi-infinite flat plate. The theory of compressible boundary layer flow has been much refined and generalized since then. Extensive reviews of the literature on this subject have been given by Stewartson [5], Gross and Dewey [6], Curle [7], Herwig [8], Kumari and Nath [9–11],van Oudheusden [12], Gersten and Herwig [13], Schlichting and Gersten [14], Hossain et al. [15] and Hossain and Pop [16].

Boundary-layer flows of gas–particle mixtures have attracted numerous experimentalists due to their wide range of applications in various problems of atmospheric, engineering and physiological fields (see [17]). In this regard, the problem related to the boundary layer flow of dilute gas–particle suspension have been investigated by many researchers, for example, [18–25]. Out of these, Singleton [20] was the first to extend the Marble's analysis [19] to compressible case where the density for both phases (carrier phase and particle phase) may vary. In this paper, the author developed the governing boundary-layer equations under the assumption of particular form of viscosity-temperature relation (i.e $\mu^*/\mu^*_\infty = (T^*/T^*_\infty)^{0.5}$) and solved the two-phase model for Stokes's relation. Based on the analysis [20], Wang and Glass

* Corresponding author.
E-mail addresses: saadiasiddiqa@gmail.com, sadia_siddiqa@ciit-attock.edu.pk (S. Siddiqa).

http://dx.doi.org/10.1016/j.amc.2016.08.037
0096-3003/

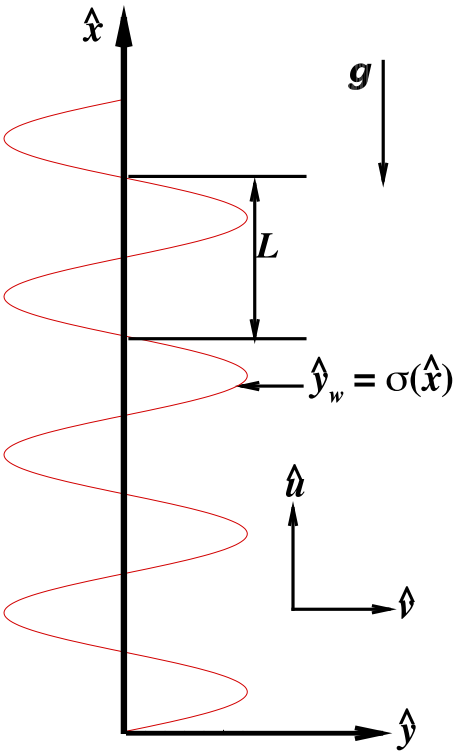

Fig. 1. Schematic of the problem.

[22] presented the more generalized form of governing equations by including the more reasonable expressions for the interaction of two-phase and the gas viscosity. In [22], the authors solved the problem of compressible dusty fluid for Stokian as well as for non-Stokian case for wide range of viscosity-temperature relation (i.e $\mu^*/\mu^*_\infty = (T^*/T^*_\infty)^\omega$; $0.5 \leq \omega \leq 1.0$, where ω being the power index).

In the present analysis, we presented the numerical solutions for compressible dusty gas along a vertical wavy surface for generalized form of temperature-viscosity relation. Owing to the complexity of the geometry of the problem and the fully compressible boundary layer equations for two-phase dusty fluid flow, a mathematical model is developed, which is possible to justify to a certain extent of physical grounds. Certain assumptions have been made to confine the influence of compressibility of carrier fluid into the boundary layer region; provided the main stream remains incompressible (i.e $\omega = \delta = 0.0$). The governing boundary equations are reduced to a convenient form by the introduction of primitive variable formulation and the resulting parabolic partial differential equations are solved by finite difference method together with Gaussian elimination technique. Numerical results of the two-phase problem are displayed in the form of wall shear stress, heat transfer rate, velocity and temperature profiles by varying several controlling parameters.

2. Analysis

Consider a vertical plate with transverse sinusoidal undulations situated in two-phase dusty fluid, as illustrated in Fig. 1. In particular, we assume that the surface profile is given by (for details see [26]):

$$\hat{y}_w = \sigma\left(\hat{x}\right) = \hat{a}\sin\left(\frac{2\pi\hat{x}}{L}\right) \tag{1}$$

where $\hat{a}$ is the amplitude of the transverse surface wave and L the characteristic length associated with the wave (over hats denote the dimensional quantities). Consideration has been given to steady, compressible dusty fluid flow and the Boussinesq approximation is employed. Both the gas and the particle cloud along the vertical wavy surface are supposed to be static at the beginning and the number density of the particles is taken as uniform throughout the flow. Another assumption is that the dust particles are spherical in shape and uniform in size so that the conservation equations given by Saffman [18] remains valid. It is assumed that the surface temperature of the vertical wavy surface, T_w, is uniform and $T_w \gg T_\infty$, where T_∞ is the ambient fluid temperature. The governing equations of the convective flow along the vertical surface can be written in dimensional form as (for details see [18,23,27]):

For the gas phase:

$$\frac{\partial(\rho\hat{u})}{\partial\hat{x}}+\frac{\partial(\rho\hat{v})}{\partial\hat{y}}=0 \tag{2}$$

$$\rho\left(\hat{u}\frac{\partial\hat{u}}{\partial\hat{x}}+\hat{v}\frac{\partial\hat{u}}{\partial\hat{y}}\right)=-\frac{\partial\hat{p}}{\partial\hat{x}}+\frac{\partial}{\partial\hat{x}}\left(\mu\frac{\partial\hat{u}}{\partial\hat{x}}\right)+\frac{\partial}{\partial\hat{y}}\left(\mu\frac{\partial\hat{u}}{\partial\hat{y}}\right)+\rho g\beta(T-T_\infty)+\frac{\rho_p}{\tau_m}(\hat{u}_p-\hat{u}) \tag{3}$$

$$\rho\left(\hat{u}\frac{\partial\hat{v}}{\partial\hat{x}}+\hat{v}\frac{\partial\hat{v}}{\partial\hat{y}}\right)=-\frac{\partial\hat{p}}{\partial\hat{y}}+\frac{\partial}{\partial\hat{x}}\left(\mu\frac{\partial\hat{v}}{\partial\hat{x}}\right)+\frac{\partial}{\partial\hat{y}}\left(\mu\frac{\partial\hat{v}}{\partial\hat{y}}\right)+\frac{\rho_p}{\tau_m}(\hat{v}_p-\hat{v}) \tag{4}$$

$$\rho c_p\left(\hat{u}\frac{\partial T}{\partial\hat{x}}+\hat{v}\frac{\partial T}{\partial\hat{y}}\right)=\frac{\partial}{\partial\hat{x}}\left(\kappa\frac{\partial T}{\partial\hat{x}}\right)+\frac{\partial}{\partial\hat{y}}\left(\kappa\frac{\partial T}{\partial\hat{y}}\right)+\frac{\rho_p c_s}{\tau_T}(T_p-T)+\frac{\rho_p}{\tau_m}\{(\hat{u}_p-\hat{u})^2+(\hat{v}_p-\hat{v})^2\} \tag{5}$$

$$\hat{p}=\rho RT \tag{6}$$

For the particle phase:

$$\frac{\partial(\rho_p\hat{u}_p)}{\partial\hat{x}}+\frac{\partial(\rho_p\hat{v}_p)}{\partial\hat{y}}=0 \tag{7}$$

$$\rho_p\left(\hat{u}_p\frac{\partial\hat{u}_p}{\partial\hat{x}}+\hat{v}_p\frac{\partial\hat{u}_p}{\partial\hat{y}}\right)=-\frac{\partial\hat{p}_p}{\partial\hat{x}}-\frac{\rho_p}{\tau_m}(\hat{u}_p-\hat{u}) \tag{8}$$

$$\rho_p\left(\hat{u}_p\frac{\partial\hat{v}_p}{\partial\hat{x}}+\hat{v}_p\frac{\partial\hat{v}_p}{\partial\hat{y}}\right)=-\frac{\partial\hat{p}_p}{\partial\hat{y}}-\frac{\rho_p}{\tau_m}(\hat{v}_p-\hat{v}) \tag{9}$$

$$\rho_p c_s\left(\hat{u}_p\frac{\partial T_p}{\partial\hat{x}}+\hat{v}_p\frac{\partial T_p}{\partial\hat{y}}\right)=-\frac{\rho_p c_s}{\tau_T}(T_p-T) \tag{10}$$

where $(\hat{u},\hat{v})$, T, $\hat{p}$, ρ, c_p, β κ, μ are respectively the velocity vector in the $(\hat{x},\hat{y})$ directions, temperature, pressure, density, specific heat at constant pressure, volumetric expansion coefficient, thermal conductivity and coefficient of viscosity of the fluid/carrier phase. Similarly, $(\hat{u}_p,\hat{v}_p)$, T_p, $\hat{p}_p$, ρ_p and c_s corresponds to the velocity vector, temperature, pressure, density and specific heat for the particle phase. Further, g is the gravitational acceleration, τ_m (τ_T) the momentum relaxation time (thermal relaxation time) for dust particles and R the gas constant. In the present analysis, a power relation for the gas viscosity μ and the thermal conductivity κ is employed as follows (see [22]):

$$\left(\frac{\mu}{\mu_\infty}\right)=\left(\frac{T-T_\infty}{T_w-T_\infty}\right)^{\omega}=\theta^{\omega} \tag{11}$$

$$\left(\frac{\kappa}{\kappa_\infty}\right)=\left(\frac{T-T_\infty}{T_w-T_\infty}\right)^{\omega}=\theta^{\omega} \tag{12}$$

where, μ_∞ and κ_∞ are respectively the dynamic viscosity and thermal conductivity of the ambient fluid and ω being the power index. The fundamental equations stated above are to be solved under appropriate boundary conditions to determine the flow field of the fluid and the dust particles. Therefore, the boundary conditions for the problem under consideration are:

At the wall of wavy surface:

$$\begin{aligned}&\hat{u}(\hat{x},\hat{y}_w)=\hat{v}(\hat{x},\hat{y}_w)=T(\hat{x},\hat{y}_w)-T_w=0\\&\hat{u}_p(\hat{x},\hat{y}_w)=\hat{v}_p(\hat{x},\hat{y}_w)=T_p(\hat{x},\hat{y}_w)-T_w=0\end{aligned} \tag{13}$$

At outer edge of boundary layer region:

$$\begin{aligned}&\hat{u}(\hat{x},\infty)=T(\hat{x},\infty)-T_\infty=0\\&\hat{u}_p(\hat{x},\infty)=T_p(\hat{x},\infty)-T_\infty=0\end{aligned} \tag{14}$$

Now, following variables are employed to make the Eqs. (2)–(14) dimensionless:

$$\begin{aligned}&(u,u_p)=\frac{\rho_\infty L}{\mu_\infty}Gr^{-1/2}(\hat{u},\hat{u}_p),\quad (v,v_p)=\frac{\rho_\infty L}{\mu_\infty}Gr^{-1/4}\big((\hat{v},\hat{v}_p)-\sigma_x(\hat{u},\hat{u}_p)\big),\quad x=\frac{\hat{x}}{L},\quad a=\frac{\hat{a}}{L}\\&y=\frac{\hat{y}-\sigma(\hat{x})}{L}Gr^{1/4},\quad (\theta,\theta_p)=\frac{(T,T_p)-T_\infty}{T_w-T_\infty},\quad (p,p_p)=\frac{L^2}{\rho_\infty\nu_\infty^2Gr}(\hat{p},\hat{p}_p),\quad \nu_\infty=\frac{\mu_\infty}{\rho_\infty}\\&\sigma_x=\frac{d\hat{\sigma}}{d\hat{x}}=\frac{d\sigma}{dx},\ \sigma(x)=\frac{\sigma(\hat{x})}{L},\ \mathrm{Pr}=\frac{\mu_\infty c_p}{\kappa_\infty},\ \bar{\rho}=\frac{\rho}{\rho_\infty},\ \bar{\mu}=\frac{\mu}{\mu_\infty},\ D_\rho=\frac{\rho_p}{\rho_\infty},\ \alpha_d=\frac{L^2}{\nu_\infty\tau_mGr^{1/2}}\\&\Delta=\frac{T_w}{T_\infty}-1,\ Gr=\frac{g\beta(T_w-T_\infty)L^3}{\nu_\infty^2},\ \gamma=\frac{c_s}{c_p},\ Ec=\frac{\nu_\infty^2Gr}{(T_w-T_\infty)c_p},\ \delta=\frac{\nu_\infty^2Grp_1}{L^2RT_\infty}\end{aligned} \tag{15}$$

By incorporating Eq. (15), the dimensional continuity, momentum and temperature equations for both phases will be transformed as:

For the gas phase:

$$\frac{\partial(\bar{\rho}u)}{\partial x}+\frac{\partial(\bar{\rho}v)}{\partial y}=0 \tag{16}$$

$$u\frac{\partial u}{\partial x}+v\frac{\partial u}{\partial y}=-\frac{\partial p}{\partial x}+\sigma_x Gr^{1/4}\frac{\partial p}{\partial y}+\left(1+\sigma_x^2\right)\frac{\partial}{\partial y}\left(\theta^{\omega}\frac{\partial u}{\partial y}\right)+\theta+D_\rho\alpha_d(u_p-u) \tag{17}$$

$$\sigma_x\left(u\frac{\partial u}{\partial x}+v\frac{\partial u}{\partial y}\right)+\sigma_{xx}u^2=-Gr^{1/4}\frac{\partial p}{\partial y}+\sigma_x\left(1+\sigma_x^2\right)\frac{\partial}{\partial y}\left(\theta^{\omega}\frac{\partial u}{\partial y}\right)+\sigma_x D_\rho\alpha_d(u_p-u) \tag{18}$$

$$u\frac{\partial\theta}{\partial x}+v\frac{\partial\theta}{\partial y}=\frac{1}{\mathrm{Pr}}\left(1+\sigma_x^2\right)\frac{\partial}{\partial y}\left(\theta^{\omega}\frac{\partial\theta}{\partial y}\right)+\frac{2}{3\mathrm{Pr}}D_\rho\alpha_d(\theta_p-\theta)+D_\rho\alpha_d Ec\{\left(1+\sigma_x^2\right)(u_p-u)^2\} \tag{19}$$

$$\delta=\bar{\rho}(1+\Delta\theta) \tag{20}$$

For the particle phase:

$$\frac{\partial(\bar{\rho}_p u_p)}{\partial x}+\frac{\partial(\bar{\rho}_p v_p)}{\partial y}=0 \tag{21}$$

$$u_p\frac{\partial u_p}{\partial x}+v_p\frac{\partial u_p}{\partial y}=-\frac{\partial p_p}{\partial x}+\sigma_x Gr^{1/4}\frac{\partial p_p}{\partial y}-\alpha_d(u_p-u) \tag{22}$$

$$\sigma_x\left(u_p\frac{\partial u_p}{\partial x}+v_p\frac{\partial u_p}{\partial y}\right)+u_p^2\sigma_{xx}=-Gr^{1/4}\frac{\partial p_p}{\partial y}-\alpha_d\sigma_x(u_p-u) \tag{23}$$

$$u_p\frac{\partial\theta_p}{\partial x}+v_p\frac{\partial\theta_p}{\partial y}=-\frac{2}{3\gamma\,\mathrm{Pr}}\alpha_d(\theta_p-\theta) \tag{24}$$

It can be observed that for $\alpha_d=0.0$, the flow is governed by natural convection in the absence of the dusty particles (i.e carrier phase only). In addition, we assume that the pressure for carrier as well as for particle phase does not vary in the stream-wise direction across the boundary layer, i.e., $p=p_p=p_1$. Thus, by elimination of $Gr^{1/4}\partial p/\partial y$ form (17) and (18) and $Gr^{1/4}\partial p_p/\partial y$ from (22) and (23), we will have the underlying form of conserved momentum equations for both phases:

$$u\frac{\partial u}{\partial x}+v\frac{\partial u}{\partial y}+\frac{\sigma_x\sigma_{xx}}{\left(1+\sigma_x^2\right)}u^2=\left(1+\sigma_x^2\right)\frac{\partial}{\partial y}\left(\theta^{\omega}\frac{\partial u}{\partial y}\right)+\frac{1}{\left(1+\sigma_x^2\right)}\theta+D_\rho\alpha_d(u_p-u) \tag{25}$$

$$u_p\frac{\partial u_p}{\partial x}+v_p\frac{\partial u_p}{\partial y}+\frac{\sigma_x\sigma_{xx}}{\left(1+\sigma_x^2\right)}u_p^2=-D_\rho\alpha_d(u_p-u) \tag{26}$$

The dimensionless form of the boundary conditions for present analysis are:

$$\begin{aligned}&u(x,0)=v(x,0)=\theta(x,0)-1=0\\&u_p(x,0)=v_p(x,0)=\theta_p(x,0)-1=0\end{aligned} \tag{27}$$

and

$$\begin{aligned}&u(x,\infty)=\theta(x,\infty)=0\\&u_p(x,\infty)=\theta_p(x,\infty)=0\end{aligned} \tag{28}$$

Now we propose to integrate the above system of equations numerically. Before applying the numerical scheme, these equations are transformed into suitable form with the help of primitive variable formulations.

3. Primitive variable formulations

To establish the solutions of the coupled Eqs. (16), (19)–(21), (24)–(26) subject to the boundary conditions (27) and (28), we switch into another system of equations with the help of following set of continuous transformations:

$$(u,u_p)=x^{\frac{1}{2}}(U,U_p),\quad (v,v_p)=x^{-\frac{1}{4}}(V,V_p),\quad (\theta,\theta_p)=(\Theta,\Theta_p),\quad y=x^{\frac{1}{4}}Y \tag{29}$$

The above mentioned set of equations will be mapped into the following set of parabolic partial differential equations:

$$\frac{1}{2}U-\frac{1}{4}Y\frac{\partial U}{\partial Y}+\frac{\partial V}{\partial Y}-\frac{\delta}{(1+\Delta\Theta)}\left(XU\frac{\partial\Theta}{\partial X}+V\frac{\partial\Theta}{\partial Y}\right)=0 \tag{30}$$

$$\left(\frac{1}{2}+\frac{X\sigma_X\sigma_{XX}}{\left(1+\sigma_X^2\right)}\right)U^2+XU\frac{\partial U}{\partial X}+\left(V-\frac{1}{4}YU\right)\frac{\partial U}{\partial Y}=\left(1+\sigma_X^2\right)\frac{\partial}{\partial Y}\left(\Theta^{\omega}\frac{\partial U}{\partial Y}\right)+\frac{1}{\left(1+\sigma_X^2\right)}\Theta$$
$$+D_\rho\alpha_d X^{1/2}(U_p-U) \tag{31}$$

$$XU\frac{\partial\Theta}{\partial X}+\left(V-\frac{1}{4}YU\right)\frac{\partial\Theta}{\partial Y}=\frac{1}{\mathrm{Pr}}(1+\sigma_X^2)\frac{\partial}{\partial Y}\left(\Theta^{\omega}\frac{\partial\Theta}{\partial Y}\right)+\frac{2}{3\mathrm{Pr}}D_\rho\alpha_d X^{1/2}(\Theta_p-\Theta)$$
$$+D_\rho\alpha_d X^{3/2}Ec(1+\sigma_X^2)(U_p-U)^2 \tag{32}$$

$$\frac{1}{2}U_p+X\frac{\partial U_p}{\partial X}-\frac{1}{4}Y\frac{\partial U_p}{\partial Y}+\frac{\partial V_p}{\partial Y}=0 \tag{33}$$

$$\left(\frac{1}{2}+\frac{X\sigma_X\sigma_{XX}}{\left(1+\sigma_X^2\right)}\right)U_p^2+XU_p\frac{\partial U_p}{\partial X}+\left(V_p-\frac{1}{4}YU_p\right)\frac{\partial U_p}{\partial Y}=-\alpha_d X^{1/2}(U_p-U) \tag{34}$$

$$XU_p\frac{\partial\Theta_p}{\partial X}+\left(V_p-\frac{1}{4}YU_p\right)\frac{\partial\Theta_p}{\partial Y}=-\frac{2}{3\gamma\,\mathrm{Pr}}\alpha_d X^{1/2}(\Theta_p-\Theta) \tag{35}$$

The boundary conditions to be satisfied are:

$$U(X,0)=V(X,0)=\Theta(X,0)-1=U_p(X,0)=V_p(X,0)=\Theta_p(X,0)-1=0$$
$$U(X,\infty)=U_p(X,\infty)=\Theta(X,0)=\Theta_p(X,\infty)=0 \tag{36}$$

The measurable physical quantities like local skin friction coefficient, τ_w, and rate of heat transfer, Q_w, are used to express the solutions of the current scenario. These quantities are much significant from an engineering point of view, as both can be served to improve many equipments in aerodynamics. The numerical values of these coefficients can be calculated from the following mathematical relations:

$$C_f=\frac{\tau_w}{\rho_\infty(\nu_\infty/L)^2},\quad Nu=\frac{LQ_w}{\kappa_\infty(T_w-T_\infty)} \tag{37}$$

where

$$\tau_w=\mu_\infty\left(\hat{\mathbf{n}}.\nabla\hat{u}\right)_{\hat{y}=0},\quad Q_w=-\kappa_\infty\left(\hat{\mathbf{n}}.\nabla T\right)_{\hat{y}=0} \tag{38}$$

Here $\hat{\mathbf{n}}$ is the unit vector normal to the wavy surface and is defined as:

$$\hat{\mathbf{n}}=\left(-\frac{\sigma_x}{\sqrt{1+\sigma_x^2}},\frac{1}{\sqrt{1+\sigma_x^2}}\right) \tag{39}$$

After some algebraic manipulations, the dimensionless expressions for skin friction and heat transfer are obtained as:

$$\tau_w=C_f\left(\frac{Gr^{-3}}{X}\right)^{1/4}=\sqrt{1+\sigma_X^2}\left(\frac{\partial U}{\partial Y}\right)_{Y=0}$$
$$Q_w=Nu\left(\frac{Gr}{X}\right)^{-1/4}=-\sqrt{1+\sigma_X^2}\left(\frac{\partial\Theta}{\partial Y}\right)_{Y=0} \tag{40}$$

The coupled system of non-linear partial differential Eqs. (30)–(36) is solved numerically by using an implicit, iterative tri-diagonal finite difference scheme. The brief description of the numerical scheme is given in Appendix A. In the next section, numerical solutions obtained from the above algorithm are graphed and discussed as well.

4. Results and discussion

The main purpose of this analysis is to understand the behavior of compressible dusty gas along a vertical wavy surface. We perform the two-dimensional simulations in order to obtain the solutions from the implicit finite difference method. Particularly, the solutions are established for the air–metal mixture. Numerical results are reported for the overall effectiveness of compressibility, mass concentration of dust particles and waviness. For verification, simulated results are compared with the published results by various authors. The comparison of the present results with the solutions of other two-dimensional boundary layer flows in certain special cases indicates a fair qualitative agreement. For instance, the solutions obtained by Yao [28] can be recovered by setting $a=0.1, 0.3$, $\mathrm{Pr}=1.0$, $\alpha_d=0.0$ and $D_\rho=0.0$. This comparison is appeared in Fig. 2. The

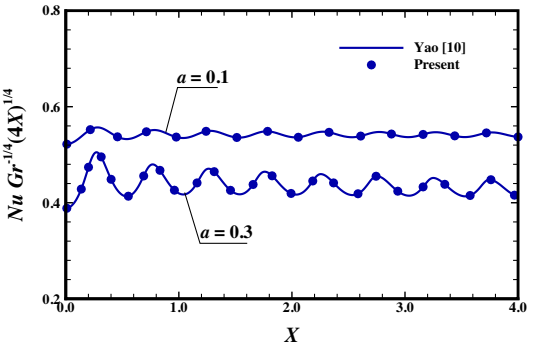

Fig. 2. Local Nusselt number coefficient for $a = 0.1, 0.3$, while $D_\rho = 0.0$, Pr $= 1.0$, $\alpha_d = 0.0$ and $\gamma = 1.0$.

Table 1
Numerical values of Q_w for $n = 0.0$, $\gamma = 0.1$, $D_\rho = 0.2$, Pr $= 5.0$, $\alpha_d = 0.5$ and $a = 0.25$

X	Q_w	
	Present	Siddiqa et al. [24]
0.0199	0.49566	0.49564
0.5095	0.51451	0.51459
1.0090	0.51398	0.51401
2.0080	0.51047	0.51047
3.0070	0.50573	0.50573
4.0060	0.50051	0.50050
5.0050	0.49508	0.49507
6.0040	0.48956	0.48955
7.0030	0.48404	0.48402
8.0020	0.47854	0.47853
9.0010	0.47311	0.47310
10.00	0.46775	0.46774

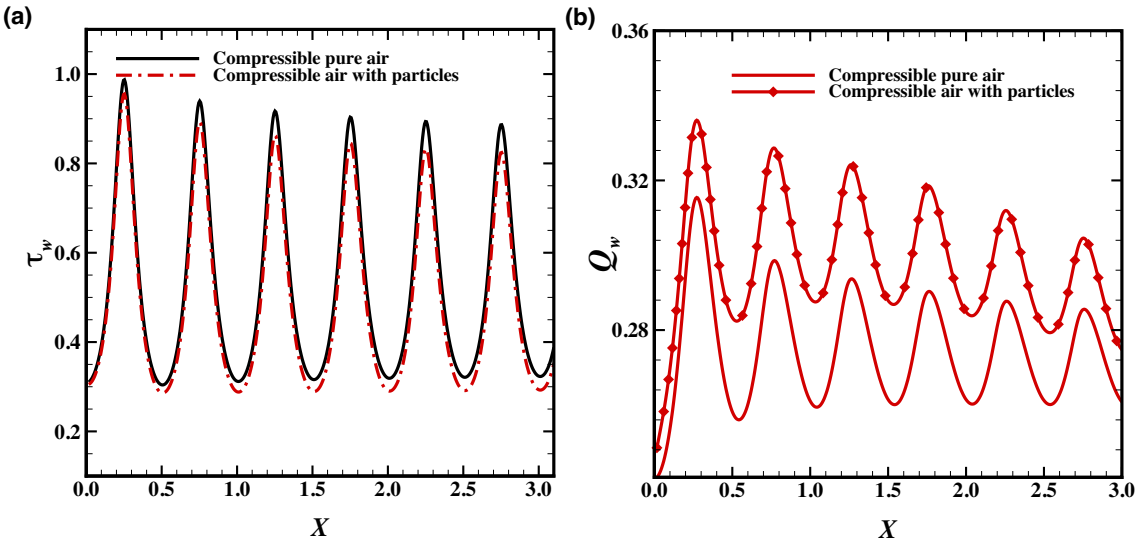

Fig. 3. (a) Skin friction and (b) Rate of heat transfer coefficients for $D_\rho = 0.0, 10.0$, while Pr $= 0.7$, $\gamma = 0.45$, $\alpha_d = 0.01$, $\omega = 0.01$, $\delta = 0.1$, $Ec = 1.0$, $\Delta = 1.1$ and $a = 0.3$.

code is further tested by comparing the solutions with Siddiqa et al. [24] in Table 1 against streamwise coordinate X. The results matches well with each other and show good accuracy.

The results for compressible air particulate suspension are represented in terms of τ_w and Q_w in Fig. 3. In this figure mass concentration parameter D_ρ characterizes the influence of particles on their surroundings. A large enhancement in the heat transfer rate (Q_w) and little reduction in the drag (τ_w) is recorded when mass concentration parameter increases.

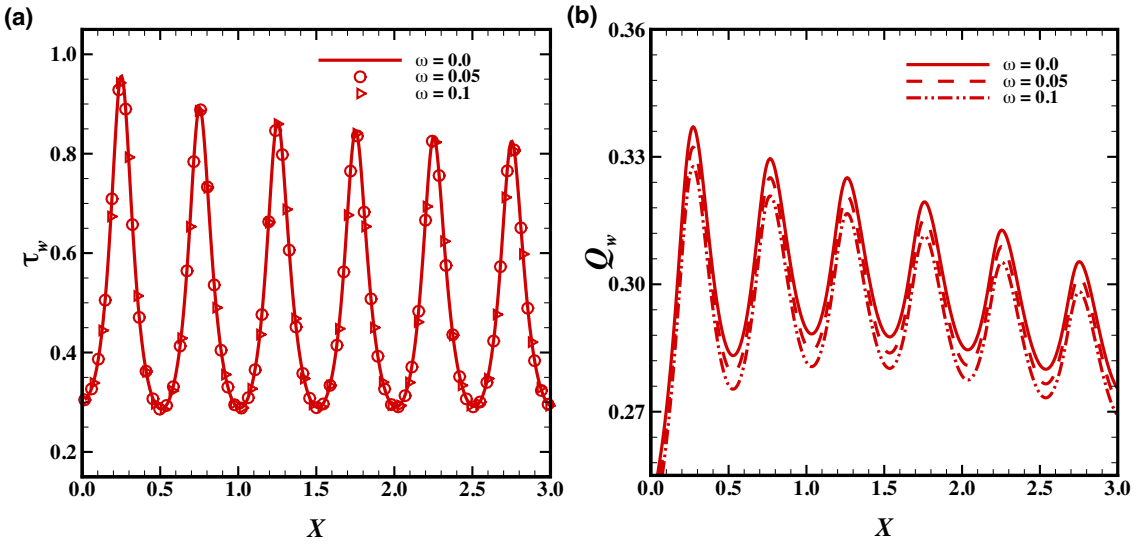

Fig. 4. (a) Skin friction and (b) Rate of heat transfer coefficients for $\omega = (0.0, 0.05, 0.1)$, while $D_\rho = 10.0$, Pr $= 0.7$, $\gamma = 0.45$, $\alpha_d = 0.01$, $\delta = 0.01$, $Ec = 1.0$, $\Delta = 1.1$ and $a = 0.3$.

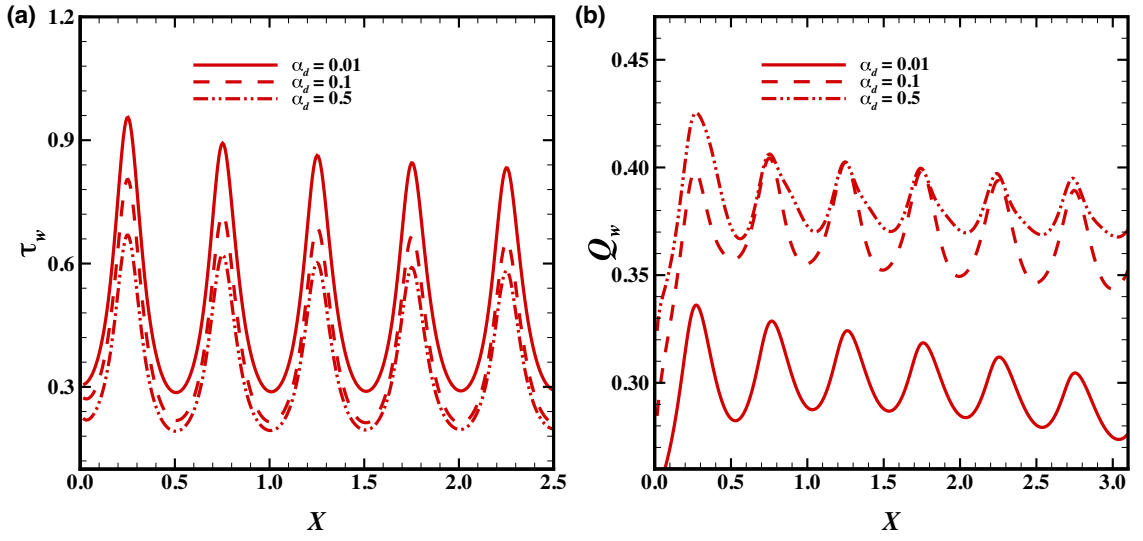

Fig. 5. (a) Skin friction and (b) Rate of heat transfer coefficients for $\alpha_d = (0.01, 0.1, 0.5)$, while $D_\rho = 10.0$, Pr $= 0.7$, $\gamma = 0.45$, $\omega = 0.01$, $\delta = 0.01$, $Ec = 1.0$, $\Delta = 1.1$ and $a = 0.3$.

Skin friction reduces because the carrier fluid loses kinetic and thermal energy, which is most likely due to the air–particle interaction and this leads to reduction of velocity of carrier fluid as compared to pure fluid case. Ultimately, the velocity gradient for the carrier fluid decreases at the surface of the plate. For the heat transfer rate, the dusty air gains some thermal energy from particles and consequently the temperature gradient for the carrier fluid increases.

The behavior of power index: ω is measured on Q_w and τ_w and is given in Fig. 4. It is observed that ω do not affect the shear stress and τ_w remain invariant for all the values of ω. But on the other hand, ω have some influence on heat transfer rate. As it can be seen from Fig. 4(b), that the rate of heat transfer is reduced for increasing values of power index ω. Such behavior is expected because the gases are more likely to variate under the influence of compressibility.

Variations in skin friction coefficient and rate of heat transfer for different values of dust parameter, α_d, is analyzed in Fig. 5. As it can be visualize from Fig. 5(a), that the skin friction is significantly reduced by increasing the value of dust parameter. By loading the dust particles in compressible gas causes the frictional forces to decline near the surface of the wavy pattern. But on the other hand, α_d has a dominating role to promote the rate of heat transfer coefficient (see Fig. 5(b)). Higher the value of dust parameter, greater will be the rate of heat transfer. The reason for such behavior may be apprehend to the fact that the presence of inert particles in compressible gas are responsible for the enhancement of

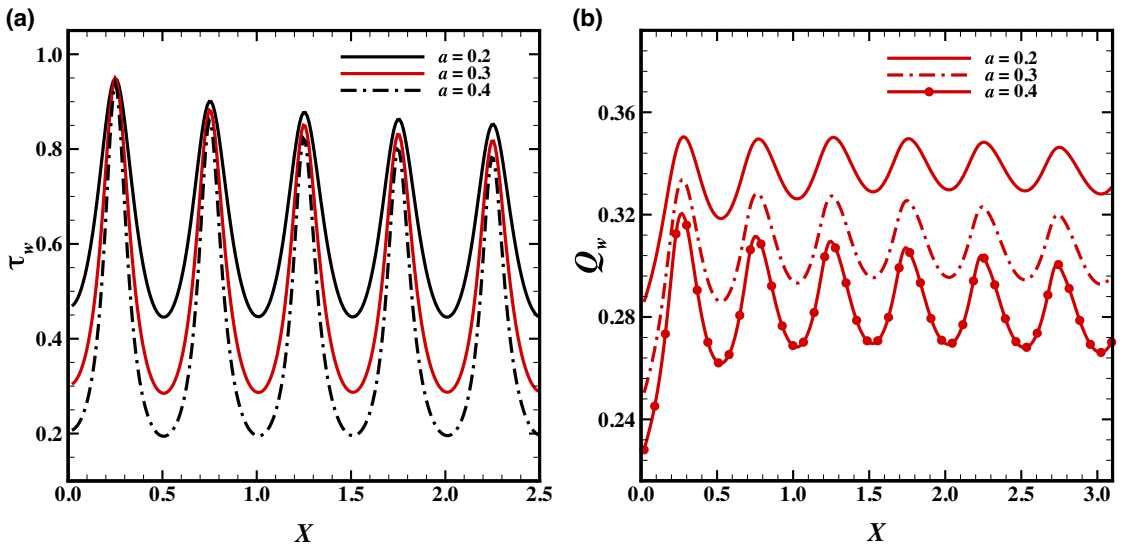

Fig. 6. (a) Skin friction and (b) Rate of heat transfer coefficients for $a = (0.2, 0.3, 0.4)$, while $D_\rho = 10.0$, $\Pr = 0.7$, $\gamma = 0.45$, $\alpha_d = 0.01$, $\omega = 0.01$, $\delta = 0.01$, $Ec = 1.0$ and $\Delta = 1.1$.

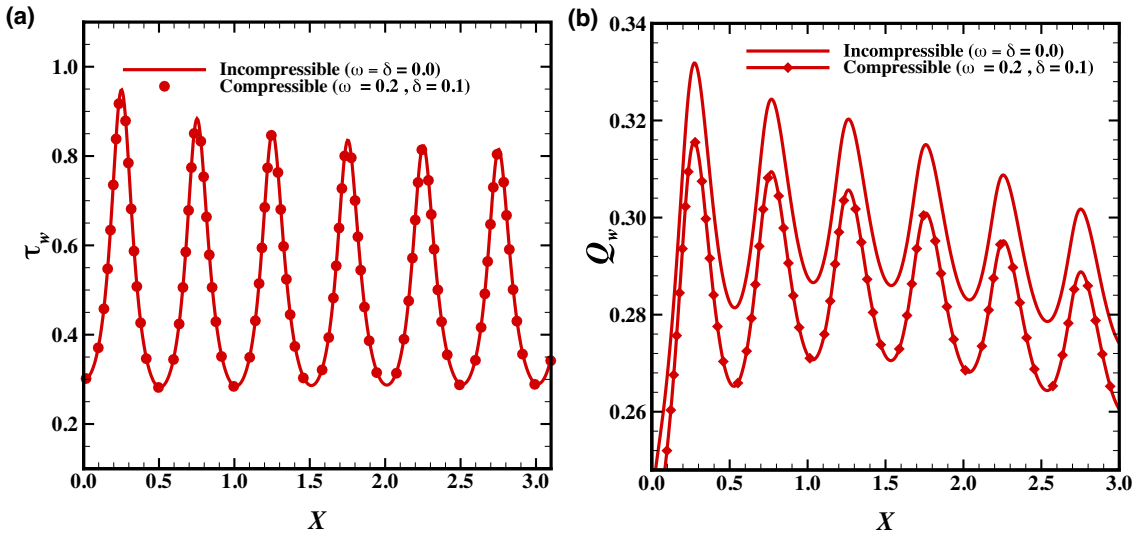

Fig. 7. (a) Skin friction and (b) Rate of heat transfer coefficients for $\omega = (0.0, 0.2)$, $\delta = (0.0, 0.1)$ while $\Pr = 0.7$, $\gamma = 0.45$, $\alpha_d = 0.01$, $D_\rho = 10.0$, $Ec = 1.0$, $\Delta = 1.1$ and $a = 0.3$.

rate of heat transfer. For large values of α_d, carrier gas will gain more thermal energy from the collision of particles, which ultimately give rise to the rate of heat transfer near the wavy geometry.

The numerical values of τ_w and Q_w for some values of amplitude of the wavy surface parameter, a, are presented through Fig. 6. The change in surface contour is followed by raise and fall of the curves. As it can be visualize from Fig. 6(a), that the influence of amplitude a, on average, is to reduce the rate of skin friction. Similar behavior is recorded for the rate of heat transfer. As a whole, the rate of heat transfer, Q_w, reduces when the amplitude of the sinusoidal waveform increases. As the amplitude increases the shape of the wave gradually changes from sinusoidal waveform to the unusual shape. The reduction in the magnitude of the temperature gradient happened due to the simultaneous influence of centrifugal and buoyancy force. Furthermore, we notice that the change in rate of heat transfer is more pronounced for larger values of the amplitude a and this factor acts as a retarding force for heat transfer coefficient.

In order to determine the influence of fluid compressibility parameters (δ and ω), Fig. 7 is plotted. It is important to mention here that, ($\delta = \omega = 0.0$) represents the model for two-phase incompressible dusty gas. As expected, the skin friction is same for both compressible and incompressible dusty gases (see Fig. 7(a)). The plots remain invariant for whole range of δ and ω. But on the other hand, it is observed from Fig. 7(b) that compressibility parameters has notable effect on

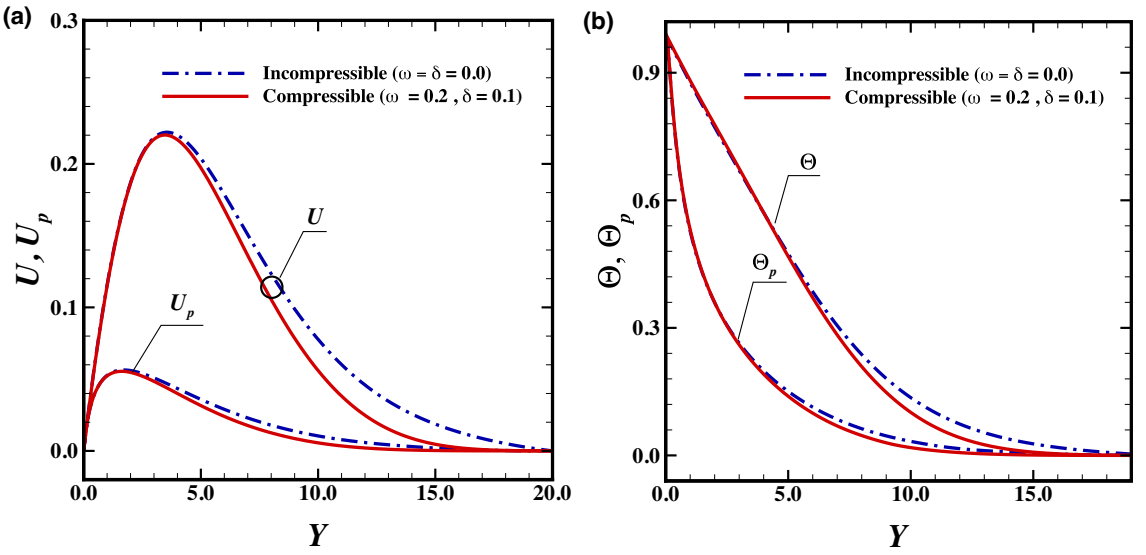

Fig. 8. (a) Velocity and (b) Temperature profile for $\omega = (0.0, 0.2)$, $\delta = (0.0, 0.1)$ while $\mathrm{Pr} = 0.7$, $\gamma = 0.45$, $\alpha_d = 0.01$, $D_\rho = 10.0$, $Ec = 1.0$, $\Delta = 1.1$ and $a = 0.3$.

heat transfer coefficient. For non-zero values of δ and ω, the rate of heat transfer is sufficiently reduced at the surface of wavy plate. Fig. 7(b) reveals the fact that the effect of compressibility of dusty gas is more likely to affect the rate of heat transfer in the boundary layer region. Such behavior is expected because increment in values of δ and ω leads to decrease the temperature of the dusty gas and ultimately Q_w becomes low in the vicinity of the uneven surface.

Representative velocity profiles and temperature profiles for carrier as well as dusty phase under the effect of parameters δ and ω are plotted in Fig. 8. As it can be seen from Fig. 8(a), that the incompressible gas (i.e, $\delta = \omega = 0.0$) acts like a supportive driving force that accelerates the air particulate suspension flow, and, as a result, the velocity for both phases, (U, U_p), within the boundary layer increases significantly. The plots for velocity profiles for both, carrier as well as particle phase, quickly attains its asymptotic value when the compressible gas is penetrated into the mechanism. Further, it is seen from Fig. 8(b) that the temperature profiles for both phases, (Θ, Θ_p), decreases when δ and ω increases. The temperature-dependent physical characteristics of the gas are responsible for this behavior as they causes an increment in temperature of the gas for both phases near the axis of the flow.

5. Conclusion

The present analysis aims to compute the numerical results of two-phase compressible dusty fluid flow moving along a vertical wavy surface. Coordinate transformations (primitive variable formulations) are applied to switch the governing equations of the carrier and the dispersed phase into another set of equations. Two-point finite difference solutions are obtained for the whole range of axial coordinate X. Numerical results give a clear insight of the response of compressible dusty gas. Effect of various emerging parameters are explored by expressing their relevance on skin friction and heat transfer rate. Velocity and temperature distributions are plotted for carrier as well as particle phase for the compressible parameters. From this analysis, it is observed that mass concentration parameter, D_ρ, and the dust parameter, α_d extensively promotes the rate of heat transfer whereas the parameters δ and ω has pronounced effect in reducing the skin friction within the boundary layer region. In addition, the velocity and temperature profiles for both phases quickly attain an asymptotic behavior when compressible air is penetrated into the mechanism.

Appendix

The discretization procedure is carried out by incorporating two-point backward difference formulae for all the first order derivatives with respect to X as:

$$\left(\frac{\partial \Omega}{\partial X}\right)_{i,j} = \frac{\Omega_{i,j} - \Omega_{i-1,j}}{\Delta X}$$

Similarly, derivatives with respect to Y are replaced by central difference quotients of the form:

$$\left(\frac{\partial \Omega}{\partial Y}\right)_{i,j} = \frac{\Omega_{i,j+1} - \Omega_{i,j-1}}{\Delta Y}$$

where

$$\Omega_{i,j} = \Omega(X_i, Y_j) \quad Y_j = (j-1)\Delta Y \quad \text{for} \quad j = 1, 2, 3 \ldots N$$

$$Y_\infty = Y_N \quad X_i = (i-1)\Delta X \quad \text{for} \quad i = 1, 2, 3 \ldots M$$

Here $\Omega_{i,j}$ denotes the dependent variable U, U_p, Θ, Θ_p, and i, j are the node locations along the X and Y directions, respectively. The system of equations is cast into a tridiagonal matrix equation of the form:

$$A_{i,j}\Omega_{i,j-1} + B_{i,j}\Omega_{i,j} + C_{i,j}\Omega_{i,j+1} = D_{i,j}$$

where

$$\Omega_{i,j} = \begin{bmatrix} U \\ \Theta \\ U_p \\ \Theta_p \end{bmatrix} \quad A_{i,j} = \begin{bmatrix} A_{11} & 0 & 0 & 0 \\ 0 & A_{22} & 0 & 0 \\ 0 & 0 & A_{33} & 0 \\ 0 & 0 & 0 & A_{44} \end{bmatrix} \quad B_{i,j} = \begin{bmatrix} B_{11} & B_{12} & B_{13} & B_{14} \\ 0 & B_{22} & B_{23} & B_{24} \\ 0 & 0 & B_{33} & B_{34} \\ 0 & 0 & 0 & B_{44} \end{bmatrix}$$

$$C_{i,j} = \begin{bmatrix} C_{11} & 0 & 0 & 0 \\ 0 & C_{22} & 0 & 0 \\ 0 & 0 & C_{33} & 0 \\ 0 & 0 & 0 & C_{44} \end{bmatrix} \quad D_{i,j} = \begin{bmatrix} D_1 \\ D_2 \\ D_3 \\ D_4 \end{bmatrix} \quad \Omega_1 = \begin{bmatrix} 0 \\ 1 \\ 0 \\ 1 \end{bmatrix} \quad \Omega_N = \begin{bmatrix} 0 \\ 0 \\ 0 \\ 0 \end{bmatrix}$$

An algorithm that can be used to obtain the solution $\Omega_{i,j}$ at a certain stream-wise distance X is given as:

$$\Omega_{i,j} = -E_{i,j}\Omega_{i,j+1} + F_{i,j} \quad 1 \le j \le N-1$$

where

$$E_1 = E_N = \begin{bmatrix} 0 & 0 & 0 & 0 \\ 0 & 0 & 0 & 0 \\ 0 & 0 & 0 & 0 \\ 0 & 0 & 0 & 0 \end{bmatrix}, \quad F_1 = \begin{bmatrix} 1 \\ 1 \\ 1 \\ 1 \end{bmatrix}, \quad F_N = \begin{bmatrix} 0 \\ 0 \\ 0 \\ 0 \end{bmatrix}$$

$$E_j = (B_j - A_j E_{j-1})^{-1} C_j \quad 2 \leqslant j \leqslant N-1$$

$$F_j = (B_j - A_j E_{j-1})^{-1} (D_j - A_j F_{j-1}) \quad 2 \leqslant j \leqslant N-1$$

Based on the information available at the ith nodal point, the dependent variables Ω_j are predicted at $i+1$th stage.

References

[1] P.H. Oosthuizen, W.E. Carscallen, Compressible Fluid Flow, McGraw-Hill, New York, 1997.
[2] G. Kuerti, The laminar boundary layer in compressible flow, Adv. Appl. Mech. 2 (1951) 21–92.
[3] A. Young, Section on boundary layers, in: L. Howarth (Ed.), Modern Developments in Fluid Mechanics High Speed Flow, 1, Clarendon Press, Oxford, 1953, pp. 375–475.
[4] F.K. Moore, Unsteady laminar boundary-layer flows, TN 2471, NACA (1951).
[5] K. Stewartson, The Theory of Laminar Boundary Layers in Compressible Fluids, Oxford University Press, 1964.
[6] A. Gross, C.F. Dewey, Similar solutions of the laminar boundary layer equations with variable fluid properties, in: W. Fiszdon (Ed.), Fluid dynamics transitions, 2, Pergamon Press, Oxford, 1965.
[7] N. Curle, Effects of a sharp pressure rise on a compressible laminar boundary layer, when the prandtl number is $\sigma = 0.72$, Proc. Roy. Soc. 84A (1979) 153–171.
[8] H. Herwing, An asymptotic approach to compressible boundary-layer flow, Int. J. Heat Mass Transf. 30 (1987) 59–68.
[9] M. Kumari, G. Nath, Self-similar solution of unsteady compressible three-dimensional stagnation-point boundary layers, J. Appl. Math. Phys. 32 (1981) 267–276.
[10] M. Kumari, G. Nath, Heat and mass transfer in unsteady compressible axisymmetric stagnation point boundary layer flow over a rotating body, Int. J. Heat Mass Transf. 25 (1982) 290–293.
[11] M. Kumari, G. Nath, Effect of large blowing rates on the compressible boundary layer flow at the stagnation point of a rotating sphere, Acta Mech. 121 (1997) 115–129.
[12] B.W. van Oudheusden, A complete crocco integral for two-dimensional laminar boundary layer flow over an adiabatic wall for prandtl numbers near unity, J. Fluid Mech. 353 (1997) 313–330.
[13] K. Gersten, H. Herwig, Strómungsmechanik, Vieweg, Braunschweig, Wiesbaden, 1992.
[14] H. Schlichting, K. Gersten, Grenzschicht-Theorie, ninth, Springer, 1997.
[15] M.A. Hossain, I. Pop, T.-Y. Na, Effect of heat transfer on compressible boundary layer flow over a circular cylinder, Acta Mech. 131 (1998) 267–272.
[16] M.A. Hossain, I. Pop, Effect of heat transfer on compressible boundary layer flow past a sphere, ZAMM Z. Angew. Math. Mech. 79 (10) (1999) 715–720.
[17] G. Rudinger, Fundamentals of Gas–Particle Flow, Elsevier Scientific Publishing Co., Amsterdam, 1980.
[18] P.G. Saffman, On the stability of laminar flow of a dusty gas, J. Fluid Mech. 13 (1962) 120–128.
[19] F.E. Marble, Dynamics of a Gas Containing Small Solid Particles, Combustion and Propulsion, Pergamon Press, 1963. 5th AGARD colloquium
[20] R.E. Singleton Ph.d. thesis, California Institute of Technology, 1964.
[21] N. Datta, S.K. Mishra, Boundary layer flow of a dusty fluid over a semi-infinite flat plate, Acta Mech. 42 (1982) 71–83.
[22] B.Y. Wang, I.I. Glass, Compressible laminar boundary-layer flows of a dusty gas over a semi-infinite flat plate, J. Fluid Mech. 186 (1988) 223–241.
[23] S. Siddiqa, M.A. Hossain, S.C. Saha, Two-phase natural convection flow of a dusty fluid, Int. J. Numer. Methods Heat Fluid Flow 45 (2015) 1542–1556.
[24] S. Siddiqa, M.N. Abrar, M.A. Hossain, M. Awais, Dynamics of two-phase dusty fluid flow along a wavy surface, Int. J. Nonlinear Sci. Numer. Simul. 17 (2016) 185–193.
[25] S. Siddiqa, N. Begum, M.A. Hossain, N. Massarotti, Influence of thermal radiation on contaminated air and water flow past a vertical wavy frustum of a cone, Int. Commun. Heat Mass 76 (2016) 63–68.

[26] S. Siddiqa, N. Begum, M.A. Hossain, Radiation effects from an isothermal vertical wavy cone with variable fluid properties, Appl. Math. Comput. 289 (2016) 149–158.
[27] S. Siddiqa, G. Hina, N. Begum, S. Saleem, M.A. Hossain, R.S.R. Gorla, Numerical and analytical solution of nanofluid bioconvection due to gyrotactic microorganisms along a vertical wavy cone, Int. J. Heat Mass Transf. 101 (2016) 608–613.
[28] L.S. Yao, Natural convection along a vertical wavy surface, J. Heat Transf. 105 (1983) 465–468.